Pulse EPR-enabled interpretation of scarce pseudocontact shifts induced by lanthanide binding tags

Elwy H. Abdelkader, Xuejun Yao, Akiva Feintuch, Luke A. Adams, Luigi Aurelio, Bim Graham, Daniella Goldfarb, Gottfried Otting*

Research School of Chemistry, Australian National University, Canberra, ACT 2601, Australia
Department of Chemical Physics, Weizmann Institute of Science, Rehovot 76100, Israel
Monash Institute of Pharmaceutical Sciences, Monash University, Parkville VIC 3052, Australia

* Corresponding author
phone: +61 2 61256508
fax: +61 2 61250750
e-mail: gottfried.otting@anu.edu.au

Keywords: double electron-electron resonance; *E. coli* aspartate/glutamate binding protein; integrative structural biology; lanthanide tag; pseudocontact shift

Abstract

Pseudocontact shifts (PCS) induced by tags loaded with paramagnetic lanthanide ions provide powerful long-range structure information, provided the location of the metal ion relative to the target protein is known. Usually, the metal position is determined by fitting the magnetic susceptibility anisotropy ($\Delta\chi$) tensor to the 3D structure of the protein in an 8-parameter fit, which requires a large set of PCSs to be reliable. In an alternative approach, we used multiple Gd^{3+}-Gd^{3+} distances measured by double electron-electron resonance (DEER) experiments to define the metal position, allowing $\Delta\chi$-tensor determinations from more robust 5-parameter fits that can be performed with a relatively sparse set of PCSs. Using this approach with the 32 kDa *E. coli* aspartate/glutamate binding protein (DEBP), we demonstrate a structural transition between substrate-bound and substrate-free DEBP, supported by PCSs generated by C3-Tm^{3+} and C3-Tb^{3+} tags attached to a genetically encoded *p*-azidophenylalanine residue. The significance of small

PCSs was magnified by considering the difference between the chemical shifts measured with Tb^{3+} and Tm^{3+} rather than involving a diamagnetic reference. The integrative sparse data approach developed in this work makes poorly soluble proteins of limited stability amenable to structural studies in solution, without having to rely on cysteine mutations for tag attachment.

Introduction

In recent years, the integration of different biophysical techniques has emerged as a highly successful approach to the study of biomacromolecular systems (Ward et al. 2013; van den Bedem and Fraser 2015). For protein structure analysis by solution NMR spectroscopy, single-crystal X-ray structures (Baldwin et al. 1991) and small-angle X-ray scattering (Sunnerhagen et al. 1996) have long been recognized to present particularly valuable complementary information. Similarly, electron paramagnetic resonance (EPR) methods have contributed much structural information about the coordination environment of metal ions and through long-range distance measurements between spin labels, but there are only few examples where distance measurements by DEER experiments have been combined with NMR data, either to supplement NMR restraints by additional DEER distance restraints (Yang et al. 2010; Yagi et al. 2011; Duss et al 2014) or to extend and correlate NMR effects with DEER data (Huang et al. 2012; Yang et al. 2013). Most of these examples employed flexible nitroxide tags. The present work integrates NMR and distance measurements by DEER experiments in a much closer manner, using the coordinates of Gd^{3+} ions identified by DEER to enable the interpretation of sparse PCSs generated by the same lanthanide binding tag, but using Tm^{3+} and Tb^{3+} instead of Gd^{3+} ions.

In previous work we used the *E. coli* aspartate/glutamate-binding protein (DEBP) as a model system to investigate the utility of pairs of C3-Gd^{3+} tags (Loh et al. 2013) to assess the 3D structure of a protein by a large number of Gd^{3+}-Gd^{3+} distances in the range of 2.5 to 6 nm measured by DEER (Abdelkader et al. 2015). A simple protocol for modelling the conformation of the tag on the protein structure proved to predict the metal coordinates associated with the tag with exceptional reliability as shown by DEER. The C3-Gd^{3+} tag was further advantageous because DEBP contains a disulfide bond. Most lanthanide tags are designed for ligation to cysteine residues (Su et al. 2010; Keizers and Ubbink 2011), which can be incompatible with disulfide bonds. No such complication applies for the C3-Gd^{3+} tag, which is attached to a *p*-azidophenylalanine (AzF) residue by Cu(I)-catalyzed click chemistry (Loh et al. 2013). AzF is an unnatural amino acid that can be site-specifically incorporated into proteins by genetic encoding, using an orthogonal amber-suppressor tRNA/aminoacyl-tRNA synthetase system (Chin et al. 2002; Young et al. 2011).

DEBP belongs to the family of periplasmic ligand binding proteins (PBP) and a crystal

structure is available of the highly homologous protein from *Shigella flexneri* with bound glutamate (Hu et al. 2008). The amino acid sequences of the *S. flexneri* and *E. coli* proteins differ in only three residues (D127N, G130D, D200E), all of which are solvent exposed. In the presence of glutamate, the Gd^{3+}-Gd^{3+} distances measured by DEER with C3-Gd^{3+} tags at six different sites were in complete agreement with the crystal structure. Furthermore, simple modelling based on the crystal structure was shown to predict, with high accuracy, five of six of the lanthanide ion positions relative to the protein. The DEER experiments also revealed, however, that the Gd^{3+}-Gd^{3+} distances were, within 2 Å, the same in the glutamate-free protein. This was unexpected, as PBPs bind their ligands between two domains linked by two β-strands, which, in most PBPs analyzed with and without ligand, mark the location of a hinge between the domains. By moving as mostly rigid entities in an open-and-shut movement, the domains can capture and release ligand (Okumoto et al. 2005). The crystal structure of the *S. flexneri* protein displays the closed state, in which glutamate is bound without solvent accessibility.

In view of the importance of glutamate as a neurotransmitter and key metabolite, DEBP has attracted much interest for the design of glutamate biosensors (de Lorimier et al. 2002; Okumoto et al. 2005; Hires et al. 2008; Marvin et al. 2013). These biosensors critically depend on a conformational change between the glutamate-bound and glutamate-free form of the protein. In the best DEBP-based glutamate sensors, however, DEBP has been modified in the hinge region between the domains (Hires et al. 2008; Marvin et al. 2013), raising the possibility that the capture and release of glutamate by wild-type DEBP involves only a local rather than global structural change.

To determine whether the closed conformation indicated by the DEER experiments of substrate-free DEBP is an artefact of the measurement conditions (DEER measurements are performed in frozen solution in the presence of 20% glycerol) or whether the closed state is also predominant in liquid solution at 25 ^{o}C, we turned to NMR spectroscopy. Unfortunately, DEBP proved to be insufficiently soluble to allow resonance assignments by conventional 3D NMR spectroscopy, precipitating over the course of hours at concentrations much above 0.1 mM. To overcome the limitations posed by the limited solubility of the protein, we set out to measure PCSs of backbone amide protons detected in ^{15}N-HSQC spectra of selectively ^{15}N-labelled samples, using the C3-tag loaded with either Tm^{3+} or Tb^{3+} ions to induce the PCSs. This approach encountered two major obstacles. First, the spectral overlap in ^{15}N-HSQC spectra of uniformly ^{15}N-labelled protein compromised resonance assignments and PCS measurements, a problem solved by combining selective ^{15}N-isotope labelling with resonance assignment by site-directed mutagenesis (the latter involving the preparation of samples, in which single-labelled residues were mutated to a different unlabelled amino acid type. Second, as site-directed mutagenesis made the assignment of a large

number of backbone amide cross-peaks laborious, only a limited number of PCSs could be measured and assigned to individual residues, rendering a reliable identification of the metal position difficult. As shown previously by Ubbink and co-workers, a lanthanide ion can be positioned at a highly predictable position by the use of a double-armed tag attached to two cysteine residues (Keizers et al. 2008), but the disulfide bond in DEBP compromises the utility of cysteine mutations. This situation prompted the current work, where we attached lanthanide ions to an AzF residue and used the metal coordinates obtained by DEER experiments to enable interpretation of the sparse PCSs. Integration of the structural information from a single-crystal X-ray structure, Gd^{3+}-Gd^{3+} distance measurements from DEER and PCSs recorded for a limited set of ^{15}N-HSQC cross-peaks provides a practical approach to structural studies of difficult proteins.

Materials and methods

Protein sample preparation

Constructs of DEBP contained an N-terminal His_6 tag followed by a tobacco etch virus (TEV) protease recognition site but was devoid of the periplasmic leader sequence (Figure S1). They were expressed using the pETMCSIII vector (Neylon et al. 2000) as described previously (Abdelkader et al. 2015). Samples were prepared by cell-free protein synthesis in a dialysis system following an established protocol (Ozawa et al. 2004; Apponyi et al. 2008). Selectively ^{15}N-labelled samples were prepared with ^{15}N-labelled valine, isoleucine and serine. To assign the respective ^{15}N-HSQC cross-peaks of these samples, valine residues were mutated to alanine or isoleucine, isoleucine residues were mutated to valine, and serine residues were mutated to alanine. All mutant samples were prepared using PCR to introduce the mutation, followed by a second round of PCR to amplify the DNA with eight-nucleotide single-stranded overhangs suitable for protein production by cell-free synthesis (Wu et al. 2007; see the Supporting Information for the primers used). Each cell-free reaction was conducted at 30 °C in a dialysis system with 2 or 3 mL inner reaction mixture and 20 or 30 mL outer buffer, respectively. ^{15}N-labelled amino acids were provided at a concentration of 1 mM.

The DEBP N146AzF mutant was produced like all other mutants, using PCR to insert an amber stop codon at the requisite site and producing the protein by cell-free synthesis, except that an S30 extract depleted of the release factor RF1 was used (Apponyi et al. 2008; Loscha et al. 2012). In addition to the usual reagents, the inner buffer contained 0.5 mg/mL total tRNA containing optimized suppressor tRNA (Young et al. 2010), prepared as described previously (Ozawa et al. 2012), and 50 μM purified *p*-cyano-*L*-phenylalanyl-tRNA synthetase (Young et al.

2011). AzF was supplied at a concentration of 1 mM.

The protein samples were purified using a Ni-NTA column and the ligation of DEBP N146AzF with either C3-Tm^{3+} or C3-Tb^{3+} tags was achieved by Cu(I)-catalyzed click-chemistry following cleavage of the His_6-tag with TEV protease as described previously (Abdelkader et al. 2015).

To remove bound glutamate, the protein samples were denatured by the addition of guanidine hydrochloride to a final concentration of 6 M. The solution was left at room temperature for 2 h. Refolding and removal of free glutamate was achieved by dialyzing against "click buffer" (50 mM sodium phosphate, pH 8, 150 mM sodium chloride) at 4°C, following a published protocol (Hu et al. 2008). Finally, the protein samples were concentrated using an Amicon ultrafiltration centrifugal tube with a molecular weight cutoff of 10 kDa. The average yield was about 1 mg of purified protein per mL cell-free reaction mixture (inner buffer). The disulfide bond between Cys88 and Cys213 formed spontaneously during the refolding reaction.

For NMR measurements, the protein samples were dialyzed against NMR buffer (50 mM sodium phosphate, pH 7.4, 150 mM sodium chloride) at 4 °C and concentrated using an Amicon ultrafiltration centrifugal tube with a molecular weight cutoff of 10 kDa. 10% D_2O was added before NMR measurement. The final samples contained about 0.1 to 0.2 mM protein. Samples of glutamate-bound DEBP were obtained by the addition of a 10-fold excess of potassium glutamate in NMR buffer.

NMR spectroscopy

All NMR spectra were recorded at 25 °C on Bruker NMR spectrometers equipped with TCI cryoprobes. The ^{15}N-HSQC spectra of the valine-to-alanine mutants were recorded at a ^{1}H NMR frequency of 600 MHz with t_{2max} = 40 ms, t_{1max} values ranging between 25 and 40 ms, and total recording times between 1 and 24 h. The N_z-exchange spectrum was recorded at a ^{1}H NMR frequency of 800 MHz in 10 h, using t_{2max} = 46 ms, t_{1max} = 20 ms, and a mixing time of 100 ms. ^{15}N-HSQC spectra of diamagnetic and C3-Tm^{3+} and C3-Tb^{3+} tagged samples were recorded with protein concentrations of about 0.15 mM at a ^{1}H NMR frequency of 800 MHz, using t_{2max} = 50 ms, t_{1max} = 25 ms, and total recording times of about 45 min for the sample without tag and without glutamate, 3 h for the sample without tag and with glutamate, and 12 h for the samples with paramagnetic tags.

Results

Resonance assignments by site-directed mutagenesis

The ^{15}N-HSQC spectrum of a selectively ^{15}N-valine-labelled sample of wild-type DEBP displayed 19 cross-peaks in the presence of glutamate, corresponding precisely to the number of valine residues in the protein. In the absence of glutamate, 18 cross-peaks were resolved (Figure 1). The protein was less prone to precipitation in the presence of glutamate. Therefore, we set out to assign the ^{15}N-HSQC cross-peaks of the valine residues of glutamate-bound DEBP by preparing 19 samples of ^{15}N-valine-labelled DEBP, in which each valine residue was mutated one by one to alanine. In seven of those mutants, the spectra changed too much to allow unambiguous assignments. In these cases, new samples were prepared in the same way, except that the valine residues were changed to isoleucine. This yielded the assignment of the ^{15}N-HSQC cross-peaks of most valine residues, except that the cross-peaks of Val133 and Val134 had similar chemical shifts (Figure 1), which were sensitive to mutation of either of these residues (Figure S9), making their resonance assignment by mutation ambiguous. The cross-peaks of these residues were assigned later by PCSs (see below). The ^{15}N-HSQC cross-peaks of Ile70 and Ile76 were also assigned by mutation, preparing the samples with ^{15}N-isoleucine and mutating the residues individually to valine (Figure S3).

Chemical exchange

To assign ^{15}N-HSQC cross-peaks of substrate-free DEBP, we recorded a heteronuclear N_z-exchange spectrum (John et al. 2007) of a sample with a sub-stoichiometric amount of glutamate. The exchange cross-peaks in this spectrum allowed the transfer of the resonance assignments between the glutamate-free and glutamate-bound form (Fig. 3). The peak intensity ratio of the exchange cross-peaks and auto-peaks indicated an exchange rate of 7 s^{-1}. The largest changes in chemical shifts were observed for V28, V109, and V110, for which the largest change in chemical environment is expected if glutamate release is associated with a separation of the small and large domains of DEBP (Fig. 4c). V109 and V110 are near the putative hinge in the two-stranded β-sheet, and the amide proton of V28 is in the large domain over 13 Å away from V109 and V110, directly facing the small domain. The chemical shifts of the other valine amide protons are much more conserved, confirming the structural conservation of the small and large domains of DEBP between the states with and without glutamate. In the crystal structure, the amides of V28, V109 and V110

are over 6.5 Å from any atom of the bound glutamate, i.e. their large changes in chemical shift upon release of glutamate are not due to a loss of direct contact with the ligand. In view of the general ligand binding mechanism of PBP proteins (Quiocho and Ledvina 1996), the chemical shift changes point to a different orientation between the small and large domains in substrate-free DEBP. This conclusion is corroborated by the PCS data discussed below.

Pseudocontact shifts and exploiting metal coordinates determined by DEER

We hypothesized that, in analogy to other PBP proteins, the small and large domains of DEBP are rigid structural units that are connected by a flexible hinge, which is marked by the two-stranded β-sheet linking the two domains (Fig. 4c). By replacing N146 by a paramagnetic AzF-C3-Tm^{3+} or AzF-C3-Tb^{3+} residue (Fig. 1), domain movements are expected to generate significant changes in inter-domain PCSs while the intra-domain PCSs in the small domain are expected to remain unchanged.

PCSs were generated in DEBP N146AzF by ligation with C3-Tm^{3+} or C3-Tb^{3+} tags (Fig. 4a and b). PCSs are through-space effects that follow the equation (Bertini et al. 2002)

$$\Delta\delta^{PCS} = 1/(12\pi r^3)[\Delta\chi_{ax}(3\cos^2\theta - 1) + 1.5\Delta\chi_{rh}\sin^2\theta\cos 2\varphi] \qquad (1)$$

where $\Delta\delta^{PCS}$ is the PCS measured in ppm, r is the distance of the nuclear spin from the metal ion, $\Delta\chi_{ax}$ and $\Delta\chi_{rh}$ are the axial and rhombic components of the magnetic susceptibility anisotropy tensor $\Delta\chi$, and θ and φ are the polar angles describing the position of the nuclear spin with respect to the principal axes of the $\Delta\chi$ tensor. We fitted the $\Delta\chi$ tensors to the coordinates of the *S. flexneri* crystal structure, which represents the substrate-bound state (Hu et al. 2008), using the PCSs observed in the presence of excess glutamate (Tables S2 and S3).

In principle, fitting a $\Delta\chi$ tensor to a protein structure involves an 8-parameter fit ($\Delta\chi_{ax}$, $\Delta\chi_{rh}$, the Euler angles α, β, and γ, and the metal coordinates x, y, and z) but obtaining reliable metal coordinates from an 8-parameter fit requires that the number of measured PCSs significantly exceed the number of parameters in the fit. For DEBP N146AzF-C3-Tm^{3+}, however, only eleven experimental PCSs were available, and the number was even smaller for DEBP N146AzF-C3-Tb^{3+} (Tables S2 and S3). To obtain a reliable $\Delta\chi$-tensor fit, we used the metal position determined previously by modelling an AzF-C3-Tm^{3+} residue at site 146, which had been confirmed by Gd^{3+}-Gd^{3+} distance measurements by DEER experiments. Using pairs of AzF-C3-Gd^{3+} residues, the DEER experiments measured five different Gd^{3+}-Gd^{3+} distances to the Gd^{3+} ion of the AzF-C3-

Gd^{3+} residue at position 146, which was part of a network of six Gd^{3+} ions with a total of 15 measured distances (Abdelkader et al. 2015). As the modelled distances and the distances experimentally measured by DEER experiments correlated within 2 Å, the metal position is known with good accuracy. Independent knowledge of the metal coordinates thus allowed a reduction in the dimensionality of the $\Delta\chi$-tensor parameter search from 8 to 5 ($\Delta\chi_{ax}$, $\Delta\chi_{rh}$ and three Euler angles).

The quality factor of the 5-parameter fits to the Tm^{3+} data was good (Fit I of Table 1) and it did not change significantly when the PCSs of V133 and V134 were excluded (Fit II of Table 1). Therefore, we retained these PCSs with the peak assignments as shown in Fig. 2 and 4 in all subsequent $\Delta\chi$-tensor fits. The established metal position explains the absence of the cross-peak of V135 in the paramagnetic samples by paramagnetic relaxation enhancements (PRE). In an unrestrained 8-parameter fit performed with the PCSs from the Tm^{3+}- labelled sample (Fit III of Table 1), the origin of the $\Delta\chi$ tensor moved by over 8 Å to a site that is in poor agreement with the DEER results, near the limit of where the metal could physically be located and requiring the additional assumption that the AzF-C3-Tm^{3+} tag assumes an energetically unfavourable conformation.

In the case of the sample with the C3-Tb^{3+} tag, additional cross-peaks became undetectable due to the increased PREs associated with Tb^{3+} (V133, V134 and V143; Fig. 4b; Bleaney 1972). Nonetheless, using the remaining eight PCSs, the magnitude of the $\Delta\chi$ tensor determined in a 5-parameter fit ($\Delta\chi_{ax}$, $\Delta\chi_{rh}$ and three Euler angles) that used the same metal position as the fit with Tm^{3+} yielded a $\Delta\chi_{ax}$ value about 50% larger than the $\Delta\chi_{ax}$ value obtained for Tm^{3+} (Table 2), in agreement with general expectations for a Tb^{3+} versus Tm^{3+} ion (de la Cruz et al. 2011).

Using the PCSs measured in the presence of glutamate, neither of the 5-parameter fits produced a PCS violation greater than 0.035 ppm and the correlations between back-calculated and experimentally measured PCSs were very good (Fig. 5). The quality of the fits confirms that, in the presence of glutamate, the structure of *E. coli* DEBP in solution is faithfully represented by the crystal structure of the *S. flexneri* homologue. Furthermore, the $\Delta\chi$-tensor fits support the metal position experimentally established by the DEER measurements (Abdelkader et al. 2015).

Effective $\Delta\chi$ tensor

It can be difficult to interpret PCSs from mobile lanthanide tags, if the motions significantly change the metal position. In the case of DEBP N146AzF ligated with C3-Tm^{3+} and C3-Tb^{3+}, mobility is indicated by the fact that the magnitude of the $\Delta\chi$ tensor is smaller than expected for a rigid C3 tag

(Loh et al. 2013). The DEER data, however, revealed a clear preference for specific sets of χ_1, χ_2 and χ_6 angles (Fig. 1), suggesting that averaging of the $\Delta\chi$ tensor arises more from reorientation of the metal complex with conserved metal coordinates than from large-amplitude displacement of the metal position. We note that more rotamers may be populated in solution than under the conditions of the DEER experiments, which involve frozen solutions and thus allow the freezing out of specific conformations. Importantly, however, even in situations where the metal moves between different positions over much greater distances than compatible with the χ_1 and χ_2 angles of the AzF-C3 residue in the present example, approximating the experimental PCSs by a single effective $\Delta\chi$ tensor can still produce meaningful results, so long as the effective tensor provides good fits of the PCSs at the sites of interest (Shishmarev and Otting 2013; Chen et al. 2014). In the present case, all PCSs showed the same sign (Tables S1 and S2). Therefore, the effective $\Delta\chi$ tensor for Tm^{3+} must be arranged in a way similar to that depicted in Figure 4c, i.e. with isosurfaces of positive value covering most of the protein. Similarly, only negative PCSs were observed with the Tb^{3+} tag. The tensors of Tables 1 and 2 fit these data very well. Independent of any knowledge of the exact $\Delta\chi$ tensor parameters, however, availability of the metal position from DEER experiments already makes the PCSs highly informative, as illustrated below for the structural transition between substrate-free and glutamate-bound DEBP.

PCS evidence for a structural change between substrate-free and glutamate-bound DEBP

A structural change between substrate-free and glutamate-bound DEBP is reflected in the quality factor *Q*, which measures the agreement between back-calculated and experimental PCSs in a $\Delta\chi$-tensor fit. While the PCS data measured with the Tm^{3+} tag in the presence of glutamate fit the crystal structure 2VHA of the *S. flexneri* homolog very well (Q = 0.06, no PCS violation greater than 0.035 ppm; Fit I of Table 1; Fig. 5a), the corresponding 5-parameter fit performed with PCSs observed in the absence of glutamate featured a larger *Q* factor of 0.10 (Fit IV of Table 1) and PCS violations as large as 0.05 ppm. This confirms that substrate-free DEBP in solution is structurally different from glutamate-bound DEBP, which is well represented by the closed conformation of the crystal structure 2VHA. The PCSs measured with the Tb^{3+} tag have less discriminative value (Q = 0.06 both in the presence and absence of glutamate; Table 2; Fig. 5b), which may be attributed to the small number of PCSs obtained with this lanthanide. Setting the χ_6 angle of the AzF-C3 residue to 0^o instead of 180^o resulted in a metal position shifted by about 4.6 Å, but the *Q* factors hardly changed in 5-parameter fits corresponding to Fits I and IV of Table 1 (Q = 0.05 and 0.09, respectively), showing that the results are insensitive to minor changes in metal position. In a

broader analysis, it is instructive to compare the PCS data between substrate-free and glutamate-bound DEBP by grouping them into intra- and inter-domain PCSs.

The general metal position established relative to DEBP in the closed conformation provides a valuable reference point for a qualitative PCS analysis. If the large and small domains of DEBP move apart in the absence of glutamate, one would expect that the intra-domain PCSs remain the same, while the inter-domain PCSs decrease. This was indeed observed (Fig. 6). The Tm^{3+} data showed that, except for the PCS of V143, all of the intra-domain PCSs were slightly larger in the absence of glutamate, indicating a slightly changed but overall conserved $\Delta\chi$ tensor. At the same time, the inter-domain PCSs dropped, especially for residues 95, 76 and 70, which are furthest from the two β-strands that define the putative hinge between the two domains (Fig. 6a and b; while the uncertainties associated with the PCSs of I70 were too large to make this change in PCS magnitude significant, the change was significant when considering 'super-PCSs' that compare the peak positions observed with Tm^{3+} and Tb^{3+}, see Fig. S4 and below.)

The Tb^{3+} data showed the same trends, with smaller inter-domain PCSs (residues 95, 76, 70 and 28) in the absence than in the presence of glutamate. Only three intra-domain PCSs were observed, which increased slightly for residues 177 and 202 but decreased for V110 in the substrate-free protein. As V110 is next to V109 at the boundary between the domains (Fig. 4c), it is plausible that V110 can be affected by the conformational transition between substrate-free and glutamate-bound protein. As discussed above, V110 is among the residues showing the largest chemical shift changes in the ^{15}N-HSQC spectrum in response to the presence or absence of glutamate.

The DEER data showed little evidence of this conformational transition, suggesting instead that the same (closed) conformation is predominantly populated in the presence and absence of glutamate (Abdelkader et al. 2015). Even though the tag at position 146 is far from the interface between small and large domain, could the changes in PCSs observed between substrate-free and glutamate-bound DEBP arise from a small change in the $\Delta\chi$ tensor rather than from a structural change of the protein? As the metal site, V143, and V28 lie almost on the same line in the closed conformation (Fig. 4c), no change in tensor magnitude or orientation can explain how the PCS of V28 could decrease when the PCS of V143 remains unchanged, so long as the metal position relative to the small domain does not change beyond the covalent constraints of the tag. Even though the decrease in the PCS of V28 is small, it is significant. In the samples tagged with Tm^{3+} and Tb^{3+}, the PCS changed by -0.025 and 0.09 ppm, respectively (Tables S2 and S3). These values are outside the estimated uncertainty in measuring the PCSs (about 0.01 ppm) derived from the signal-to-noise dependent accuracy with which peak positions can be determined in NMR spectra (Kontaxis et al. 2000).

Super-PCSs

PCSs are conventionally measured as chemical shift differences between paramagnetic and diamagnetic samples, but it is also possible to define "super-PCSs" as the difference in chemical shifts between two paramagnetic samples. So long as the different metal ions are located at the same position relative to the protein and the individual $\Delta\chi$ tensors are of the same size, a difference $\Delta\chi$-tensor can be fitted to the super-PCSs, which is a tensor sum of the individual $\Delta\chi$ tensors of the different metal ions, in complete analogy to the additivity of alignment tensors produced by simultaneous paramagnetic and steric alignment (Barbieri et al. 2002). In the case of DEBP N146AzF-C3 loaded with Tm^{3+} or Tb^{3+}, the individual $\Delta\chi$ tensors did not have the same size (Tables 1 and 2) and we used the super-PCSs for qualitative analysis rather than attempting to fit a difference $\Delta\chi$-tensor. In contrast to the measurements of conventional PCSs, which used untagged protein as the diamagnetic reference, the super-PCSs had the added benefit of comparing two tagged proteins that are chemically identical apart from the identity of the lanthanide ion. Furthermore, use of a diamagnetic tag such as, e.g., C3-Y^{3+}, is useful only if the ligation yields are sufficiently high to avoid overlap between the peaks from tagged and untagged protein. Most important, the ^{15}N-HSQC cross-peaks moved in opposite directions in the samples labelled with Tm^{3+} or Tb^{3+}, making the corresponding super-PCSs larger than the individual PCSs. In particular, the super-PCS of V28 s greater than 0.1 ppm, i.e. ten-fold greater than the estimated uncertainty in peak position. While the presence of paramagnetic lanthanide tags broadened the peaks of I70 and I76, obscuring their exact PCS values, the super-PCSs of both residues were clearly smaller in the absence than in the presence of glutamate (Fig. S4). All available NMR data thus indicate that a structural change occurs between substrate-free and glutamate-bound DEBP, which involves a displacement of the small and large domains of the protein relative to each other.

Evidence for domain movements in the substrate-free protein

While the PCSs indicate a conformational change between the substrate-free and glutamate-bound forms of DEBP, it proved difficult to model a single conformation that explains the smaller inter-domain PCSs of substrate-free DEBP. To assess the domain interface for mobility, we inspected Ser72 and Ser90. Both are located at the domain interface lining the ligand binding site. We assigned the ^{15}N-HSQC cross-peaks of Ser72 and Ser90 by mutation to alanine (Fig. S5). Both

cross-peaks were weak in the absence of glutamate, suggesting line broadening by chemical exchange. This points to inter-domain movements in substrate-free DEBP.

Discussion

Large proteins are difficult to analyse by solution NMR spectroscopy not only because of signal overlap and broad line widths, but also because of a tendency for reduced solubility (if measured in terms of molarity). It is thus attractive to extract structural information from lanthanide-generated PCSs observed in sensitive and well-resolved ^{15}N-HSQC spectra, especially as PCSs can report on conformations far from the tagging site, minimizing the possibility that the site of interest is perturbed by the probe. ^{15}N-HSQC spectra can be recorded of selectively ^{15}N-labelled samples and assigned by site-directed mutagenesis. In contrast to residual dipolar couplings, which are highly sensitive to local changes in bond orientations and, with only few backbone amides assigned, are difficult to interpret in terms of global structural changes, the distance dependence of PCSs offers a much clearer probe of inter-domain movements. The interpretation of PCSs, however, depends critically on the knowledge of the metal position, which, in the case of the AzF-C3-Ln^{3+} tag, can readily be obtained from modelling and DEER experiments.

Determining the location of the metal ion

The C3-tag is ideal for site-specific attachment of lanthanides in large proteins, as the tag can be ligated with AzF in a Cu(I)-catalyzed click reaction and, in contrast to established lanthanide tags, is independent of the presence of cysteine residues (Loh et al. 2013). Furthermore, recent DEER measurements performed with DEBP showed that the conformation of an AzF-C3-Ln^{3+} residue that projects into solution can be accurately predicted from the structural context of the neighbouring residues by using the mutation tool of PyMOL (DeLano 2002) and assuming that the χ_6 angle is 180^o while the lanthanide ion is coordinated by the nearest nitrogen atom of the triazole ring (Fig. 1; Abdelkader et al. 2015).

An important question is whether the positions of the Gd^{3+} ions identified in frozen solution by DEER experiments are the same as in liquid solution at ambient temperature. DEER experiments invariably yield distance distributions rather than single distances, reflecting at least in part the

conformational variability of the tag and protein. We usually model Gd^{3+}-Gd^{3+} distance distributions by a simple rotamer library approach, in which all rotatable bonds are allowed to vary within a band around preferential staggered conformations, without taking into account explicit energy terms other than disallowing van der Waals clashes with the protein (Yagi et al. 2011). The distribution peak maxima determined in this way usually agree very closely (within a couple of Å) with DEER measurements. As small energy differences between different conformations would matter even less at room temperature, the distances derived from the maximum of the distance distributions measured in the frozen state are very likely maintained in liquid solution. The validity of this assumption is supported by recent molecular dynamics simulations of molecules without tag at about 300 K, which were combined with rotamers of the metal tag based on the accessible space. Very good agreement between the DEER-derived distance distribution and the calculated one was obtained for both Gd^{3+}-Gd^{3+} distances in double-tagged DNA (Song et al. 2011) and Mn^{2+}-Mn^{2+} distances in a helical peptide (Ching et al. 2015).

The AzF-C3-Gd^{3+} residue is unusual in that the maximum of the Gd^{3+}-Gd^{3+} distance distribution can be predicted by a single tag conformation (Abdelkader et al. 2015). While the χ_1 and χ_2 angles of the AzF residue likely remain restrained at room temperature, a solvent-exposed tag would show fast rotations about the bond defined by the χ_6 angle. In the present work, we assumed that the rotamer with $\chi_6 = 180^o$, which was identified as predominant by DEER experiments, remains the most highly populated rotamer. Between the cases of $\chi_6 = 0^o$ and 180^o, the metal would be displaced by only about 4.6 Å. This is a much smaller displacement than for conventional cysteine-bound lanthanide tags (Shishmarev and Otting 2013; Abdelkader et al. 2016).

The number of DEER measurements required to locate a lanthanide ion relative to the protein of interest depends on the agreement found between the modelled positions and the experimental Gd^{3+}-Gd^{3+} distance measurements. In general, if three distance measurements with a specific AzF-C3-Gd^{3+} residue agree with the expected distances obtained by modelling, the modelled lanthanide position can be considered to be highly reliable. In the case of DEBP, only one out of six sites with AzF-C3-Gd^{3+} residues positioned the lanthanide at an unexpected site, which could be attributed to specific binding of the metal complex to the protein (Abdelkader et al. 2015). If the initial modeling fails to reproduce the measured distances, additional sites would need to be tagged and distances measured to identify the site(s), where modelling delivers the wrong answer. This could be cumbersome, as each DEER distance measurement requires a new double-tagged protein sample. In general, however, the requirement of as few as three samples with Gd^{3+} tags is an attractive alternative to producing the multitude of selectively isotope-labelled samples required to assign sufficient NMR signals by site-directed mutagenesis to enable the metal position to be reliably determined by a full 8-parameter $\Delta\chi$-tensor fit.

Conformational equilibria of substrate-free DEBP

The equilibrium between open and closed conformations of *E. coli* periplasmic ligand binding proteins has previously been investigated by solution NMR spectroscopy for the maltose binding protein (Tang et al. 2007), the glutamine binding protein (Bermejo et al. 2010), the histidine binding protein (Chu et al. 2013), the siderophore binding protein (Chu et al. 2014), and the ribose and glucose/galactose binding proteins (Ortega et al. 2012). In the absence of cognate substrates, the different proteins display very different equilibria between open and closed conformations, ranging from exclusively open conformations to relative domain orientations that are virtually identical to those of the glutamate-bound form. In many cases, the substrate-free protein showed evidence for the co-existence of open and closed conformations.

In the case of DEBP, the PCSs confirm that the glutamate-bound protein assumes the closed structure observed in the crystal structure of the *S. flexneri* homologue. In contrast to the DEER data, which indicated that the closed conformation is predominantly populated even in the absence of glutamate (Abdelkader et al. 2015), the changes in chemical shifts as well as PCSs indicate that the transition to the substrate-free protein involves a movement of the domains as rigid entities relative to each other. As the DEER experiments involved frozen solutions in the presence of 20% glycerol to prevent ice crystal formation, it is quite possible that the EPR conditions masked subtle conformational equilibria present at room temperature. In at least one other example, scarce PCSs measured in solution contradicted low-temperature EPR measurements (Skinner et al. 2015). To investigate the possibility of a preference for the closed conformation at low temperatures, we measured a ^{15}N-HSQC spectrum of the glutamate-free wild-type protein (labelled with ^{15}N-valine) at 4 ^{o}C, but found no evidence for a change in chemical shifts towards those of the closed conformation. Similarly, the addition of 20% glycerol did not indicate an increase in the population of the closed state at 25 ^{o}C.

Different scenarios can be considered to try and reconcile the DEER and NMR data of substrate-free DEBP. (i) The substrate-free protein populates a range of conformations that, on average, yield the same DEER distances as the closed state. This is unlikely, as the peak maxima of the inter-domain DEER distance distributions were highly reproducible between samples with and without glutamate, with less than 2 Å deviation and not showing any trend towards, on average, longer distances. Therefore, we assume that the closed conformation exists in equilibrium with one or more open conformations. (ii) The closed state is in equilibrium with an open conformation that is less populated than the closed conformation. In DEER data, conformations with populations

below ~25% may be difficult to detect unambiguously. Such a small population of an open conformation, however, is difficult to reconcile with the significant drop in inter-domain PCSs compared with the closed state. In practice, the inter-domain PCSs would have to change sign in the open state, which is unlikely as a dramatic structural change would be required, considering that the $\Delta\chi$-tensor orientations found in the closed state produce the same PCS sign for all valine residues (Fig. 4c). (iii) The closed state is less highly populated at room temperature than under the frozen glass conditions used for DEER measurements, and in equilibrium with one or several open conformations that, on average, yield smaller PCSs. In this case, the PCSs would indicate a greater average distance of the large domain from the tag at room temperature compared to the frozen state. Alternatively, inter-domain PCSs could be reduced by lateral movements of the large domain relative to the small domain without much opening of the domain interface. Inter-domain movements in the substrate-free state are supported by the line broadening observed for residues at the domain interface.

For a rapid structural equilibrium where only a single set of averaged NMR peaks can be observed, the first approximation would be to interpret the data by a single average conformation. If alternative conformations are available from either crystallography, molecular dynamics simulations or modelling, it is also possible to interpret the PCS data by conformational ensembles, as has been demonstrated in an exemplary manner for calmodulin and complexes thereof with different peptides (Bertini et al. 2004; Bertini et al. 2010; Dasgupta et al. 2011; Nagulapalli et al. 2012; Russo et al. 2013; Andrałojć et al. 2014). In the case of substrate-free DEBP, modelling of the substrate-free state by multiple structures is difficult in the absence of good structural models and significantly more experimental data.

Conclusion

PCSs induced by paramagnetic lanthanide tags are ideally suited to detect structural rearrangements between rigid domains, as they deliver long-range structural information across the domain interface. In the case of the *E. coli* aspartate/glutamate binding protein, all available NMR information indicates that the release of glutamate is accompanied by a global rather than local change in structure, involving movements of the N- and C-terminal domains relative to each other. This work demonstrates how the confluence of several modern techniques make the analysis by PCSs practical for a 32 kDa protein of limited solubility. Preparation of the large number of selectively isotope-labelled samples required for resonance assignment by site-directed mutagenesis is economical by cell-free protein synthesis (Torizawa et al. 2004), especially since PCR-amplified

DNA can be used directly without prior sequencing (Wu et al. 2007), and facile removal of the release factor RF1 from the cell-extract enables high incorporation yields of unnatural amino acids (AzF in the present work; Loscha et al. 2012). The present work highlights the fact that even scarce PCS data can already reveal the telltale signs of global changes in conformation. Moreover, determination of the metal position, which is of critical importance for drawing structural conclusions from PCSs, is greatly facilitated by an integrative approach, which combines the PCSs with the exceptional capacity of the AzF-C3-Ln^{3+} tag to be modelled with high accuracy, as well as with experimental verification of the metal position by a small number of distances measured by DEER experiments.

Acknowledgement

We thank Professor Peter G. Schultz and Dr. Colin C. Jackson for genes of the orthogonal tRNA/aminoacyl-tRNA synthetase system and DEBP, respectively, and Dr. Ruhu Qi for help with primer design. Financial support by the Australian Research Council (ARC) and an Australia-Weizmann Making Connections grant is gratefully acknowledged. B. G. thanks the ARC for a Future Fellowship. In part, this research was made possible by the historic generosity of the Harold Perlman family. D. G. holds the Erich Klieger professorial chair in Chemical Physics.

References

Abdelkader EH, Feintuch A, Yao X, Adams LA, Aurelio L, Graham B, Goldfarb D, Otting G (2015) Protein conformation by EPR and NMR spectroscopy using lanthanide tagging of genetically encoded amino acids. Chem Commun 51:15898–15901

Abdelkader EH, Lee MD, Feintuch A, Ramirez Cohen M, Swarbrick JD, Otting G, Graham B, Goldfarb D (2016) A new Gd^{3+} spin label for Gd^{3+}-Gd^{3+} distance measurements in proteins produces narrow distance distributions. submitted

Andrałojć W, Luchinat C, Parigi G, Ravera E (2014) Exploring regions of conformational space occupied by two-domain proteins. J Phys Chem B 118, 10576–10587

Apponyi MA, Ozawa K, Dixon NE, Otting G (2008) Cell-free protein synthesis for analysis by NMR spectroscopy. In: Kobe B, Guss M, Huber T (eds) Methods in molecular biology 426, structural proteomics: high-throughput methods. Humana Press, Totowa, pp 257–268

Baldwin ET, Weber IT, St Charles R, Xuan JC, Appella E, Yamada M, Matsushima K, Edwards BF, Clore GM, Gronenborn AM (1991) Crystal structure of interleukin 8: symbiosis of NMR and crystallography. Proc Natl Acad Sci USA 88:502–506

Barbieri R, Bertini I, Lee Y-M, Luchinat C, Velders AH (2002) Structure-independent cross-validation between dipolar couplings originating from internal and external orienting media. J Biomol NMR 22:365–368

Bermejo GA, Strub MP, Ho C, Tjandra N (2010) Ligand-free open–closed transitions of periplasmic binding proteins: the case of glutamine-binding protein. Biochemistry 49:1893–1902

Bertini I, Del Bianco C, Gelis I, Katsaros N, Luchinat C, Parigi G, Peana M, Provenzani A, Zoroddu MA (2004) Experimentally exploring the conformational space sampled by domain reorientation in calmodulin. Proc Natl Acad Sci USA 101:6841–6846

Bertini I, Giachetti A, Luchinat C, Parigi G, Petoukhov MV, Pierattelli R, Ravera E, Svergun DI (2010) Conformational space of flexible biological macromolecules from average data. J Am Chem Soc 132:13553−13558

Bertini I, Luchinat C, Parigi G (2002) Magnetic susceptibility in paramagnetic NMR. Prog NMR Spectr 40:249–273

Bleaney B (1972) Nuclear magnetic resonance shifts in solution due to lanthanide ions. J Magn Reson 8:91–100

Chen WN, Loscha KV, Nitsche C, Graham B, Otting G (2014) The dengue virus NS2B-NS3 protease retains the closed conformation in the complex with BPTI. FEBS Lett 588:2206–2211

Chin JW, Santoro SW, Martin AB, King DS, Wang L, Schultz PG (2002) Addition of p-azido-L-phenylalanine to the genetic code of Escherichia coli. J Am Chem Soc 124:9026–9027

Ching HYV, Demay-Drouhard P, Bertand HC, Policar C, Tabares LC, Un S (2015) Nanometric distance measurements between Mn(II)DOTA centers. Phys Chem Chem Phys, DOI: 10.1039/C5CP03487F

Chu BCH, DeWolf T, Vogel HJ (2013) Role of the two structural domains from the periplasmic Escherichia coli histidine-binding protein HisJ. J Biol Chem 288:31409–31422

Chu BCH, Otten R, Krewulak KD, Mulder FAA, Vogel HJ (2014) The solution structure, binding properties, and dynamics of the bacterial siderophore-binding protein FepB. J Biol Chem 289:29219–29234

Dasgupta S, Hu X, Keizers PH, Liu WM, Luchinat C, Nagulapalli M, Overhand M, Parigi G, Sgheri L, Ubbink M (2011) Narrowing the conformational space sampled by two-domain proteins with paramagnetic probes in both domains. J Biomol NMR 51:253–263

de la Cruz L, Nguyen THD, Ozawa K, Shin J, Graham B, Huber T, Otting G (2011) Binding of low-molecular weight inhibitors promotes large conformational changes in the dengue virus NS2B-NS3 protease: fold analysis by pseudocontact shifts. J Am Chem Soc 133:19205–19215

DeLano WL (2002) The PyMOL molecular graphics system. Palo Alto, CA, USA

de Lorimier RM, Smith JJ, Dwyer MA, Looger LL, Sali KM, Paavola CD, Rizk SS, Sadigov S, Conrad DW, Loew L, Hellinga HW (2002) Construction of a fluorescent biosensor family. Protein Sci 11:2655–2675

Duss O, Yulikov M, Jeschke G, Allain FH (2014) EPR-aided approach for solution structure determination of large RNAs or protein-RNA complexes. Nat Commun 5:3669

Hires SA, Zhu Y, Tsien RY (2008) Optical measurement of synaptic glutamate spillover and reuptake by linker optimized glutamate-sensitive fluorescent reporters. Proc Natl Acad Sci USA 105:4411–4416

Hu Y, Fan CP, Fu G, Zhu D, Jin Q, Wang DC (2008) Crystal structure of a glutamate/aspartate binding protein complexed with a glutamate molecule: structural basis of ligand specificity at atomic resolution. J Mol Biol, 382:99–111

Huang X, de Vera IMS, Veloro AM, Blackburn ME, Kear JL, Carter JD, Rocca JR, Simmerling C, Dunn BM, Fanucci GE (2012) Inhibitor-induced conformational shifts and ligand-exchange dynamics for HIV-1 protease measured by pulsed EPR and NMR spectroscopy. J Phys Chem B 116:14235–14244

John M, Headlam M, Dixon NE, Otting G (2007) Assignment of paramagnetic ^{15}N-HSQC spectra by heteronuclear exchange spectroscopy. J Biomol NMR 37:43–51

Keizers PHJ, Saragliadis A, Hiruma Y, Overhand M, Ubbink M (2008) Design, synthesis, and evaluation of a lanthanide chelating protein probe: CLaNP-5 yields predictable paramagnetic effects independent of environment. J Am Chem Soc 130:14802–14812

Keizers PHJ, Ubbink M (2011). Paramagnetic tagging for protein structure and dynamics analysis. Prog Nucl Magn Reson Spectrosc 58:88–96

Kontaxis G, Clore GM, Bax A (2000) Evaluation of cross-correlation effects and measurement of one-bond couplings in proteins with short transverse relaxation times. J Magn Reson 143:184–196

Loh CT, Ozawa K, Tuck K, Barlow N, Huber T, Otting G, Graham B (2013) Lanthanide tags for site-specific ligation to an unnatural amino acid and generation of pseudocontacts shifts in proteins. Bioconjugate Chem 24:260–268

Loscha KV, Herlt AJ, Qi R, Huber T, Ozawa K, Otting G (2012) Multiple-site labeling of proteins with unnatural amino acids. Angew Chem Int Ed 51:2243–2246

Marvin JS, Borghuis BG, Tian L, Cichon J, Harnett MT, Akerboom J, Gordus A, Renninger SL, Chen TW, Bargmann CI, Orger MB, Schreiter ER, Demb JB, Gan WB, Hires SA, Looger LL (2013) An optimized fluorescent probe for visualizing glutamate neurotransmission. Nat Methods 10:162–170

Nagulapalli M, Parigi G, Yuan J, Gsponer J, Deraos G, Bamm VV, Harauz G, Matsoukas J, de Planque MRR, Gerothanassis IP, Babu MM, Luchinat C, Tzakos AG (2012) Recognition pliability is coupled to structural heterogeneity: a calmodulin intrinsically disordered binding region complex. Structure 20:522–533

Neylon C, Brown SE, Kralicek AV, Miles CS, Love CA, Dixon NE (2000) Interaction of the Escherichia coli replication terminator protein (Tus) with DNA: a model derived from DNA-binding studies of mutant proteins by surface plasmon resonance. Biochemistry 39:11989 11999

Okumoto S, Looger LL, Micheva KD, Reimer RJ, Smith SJ, Frommer WB (2005) Construction and optimization of a family of genetically encoded metabolite sensors by semirational protein engineering. Proc Natl Acad Sci USA 102:8740–8745

Ortega G, Castaño D, Diercks T, Millet O (2012) Carbohydrate affinity for the glucose–galactose binding protein is regulated by allosteric domain motions. J Am Chem Soc 134:19869–19876

Ozawa K, Headlam MJ, Schaeffer PM, Henderson BR, Dixon NE, Otting G (2004) Optimization of an Escherichia coli system for cell-free synthesis of selectively ^{15}N-labelled proteins for rapid analysis by NMR spectroscopy. Eur J Biochem 271:4084–4093

Ozawa K, Loscha KV, Kuppan KV, Loh CT, Dixon NE, Otting G (2012) High-yield cell-free protein synthesis for site-specific incorporation of unnatural amino acids at two sites. Biochem Biophys Res Commun 418:652–656

Quiocho FA, Ledvina PS (1996) Atomic structure and specificity of bacterial periplasmic receptors for active transport and chemotaxis: Variation of common themes. Molec Microbiol 20:17–25

Russo L, Maestre-Martinez, Wolff S, Becker S, Griesinger C (2013) Interdomain dynamics explored by paramagnetic NMR. J Am Chem Soc 135:17111–17120

Schmitz C, Stanton-Cook MJ, Su XC, Otting G, Huber T (2008) Numbat: an interactive software tool for fitting $\Delta\chi$-tensors to molecular coordinates using pseudocontact shifts. J Biomol NMR 41:179–189

Shishmarev D, Otting G (2013) How reliable are pseudocontact shifts induced in proteins and ligands by mobile paramagnetic metal tags? A modelling study. J Biomol NMR 56:203–216

Skinner SP, Liu WM, Hiruma Y, Timmer M, Blok A, Hass MAS, Ubbink M (2015) Delicate conformational balance of the redox enzyme cytochrome P450cam. Proc Natl Acad Sci 112:9022–9027

Song Y, Meade TJ, Astashkin AV, Klein EL, Enemark JH, Raitsimring A (2011) Pulsed dipolar spectroscopy distance measurements in biomacromolecules labeled with Gd(III) markers. J Magn Reson 210:59–68

Su XC, Otting G (2010) Paramagnetic labelling of proteins and oligonucleotides for NMR. J Biomol NMR 46:101–112

Sunnerhagen M, Olah GA, Stenflo J, Forsen S, Drakenberg T, Trewhella J (1996) The relative orientation of Gla and EGF domains in coagulation factor X is altered by Ca^{2+} binding to the first EGF domain. A combined NMR small angle X-ray scattering study. Biochemistry 35:11547–11559

Tang C, Schwieters CD, Clore GM (2007) Open-to-closed transition in apo maltose-binding protein observed by paramagnetic NMR. Nature 449:1078–1082

Torizawa T, Shimizu M, Taoka M, Miyano H, Kainosho M (2004) Efficient production of isotopically labeled proteins by cell-free synthesis: a practical protocol. J Biomol NMR 30:311–325

van den Bedem H, Fraser JS (2015) Integrative, dynamic structural biology at atomic resolution – it's about time. Nat Methods 12:307–318

Ward AB, Sali A, Wilson IA (2013) Integrative structural biology. Science 339:913–915

Wu PSC, Ozawa K, Lim SP, Vasudevan S, Dixon NE, Otting G (2007) Cell-free transcription/translation from PCR amplified DNA for high-throughput NMR studies. Angew Chem Int Ed 46:3356–3358

Yagi H, Banerjee D, Graham B, Huber T, Goldfarb D, Otting G (2011) Gadolinium tagging for high-precision measurements of 6 nm distances in protein assemblies by EPR. J Am Chem Soc 133:10418–10421

Yang Y, Ramelot TA, McCarrick RM, Ni S, Feldmann EA, Cort JR, Wang H, Ciccosanti C, Jiang M, Janjua H, Acton TB, Xiao R, Everett JK, Montelione GT, Kennedy MA (2010) Combining

NMR and EPR methods for homodimer protein structure determination. J Am Chem Soc 132:11910–11913

Yang Y, Ramelot TA, McCarrick RM, Ni S, McCarrick RM, Kennedy MA (2013) Measurement of rate constants for homodimer subunit exchange using double electron-electron resonance and paramagnetic relaxation enhancements. J Biomol NMR 55:47–58

Young DD, Young TS, Jahnz M, Ahmad I, Spraggon G, Schultz PG (2011) An evolved aminoacyl-tRNA synthetase with atypical polysubstrate specificity. Biochemistry 50:1894–1900

Young TS, Ahmad I, Yin JA, Schultz PG (2010) An enhanced system for unnatural amino acid mutagenesis in E. coli. J Mol Biol 395:361–374

Figure legends

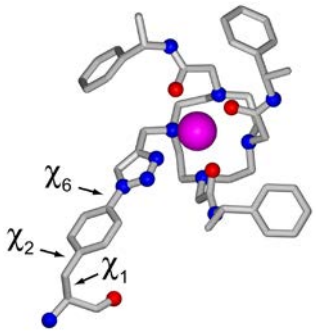

Fig. 1 Chemical structure of the AzF-C3-lanthanide residue used in the present work to tag DEBP with either Tm^{3+} or Tb^{3+}. Nitrogen, oxygen, and gadolinium atoms are shown as blue, red and magenta spheres, respectively. The dihedral angle χ_6 is 180°. The lanthanide ion is coordinated by the nitrogens of the cyclen ring, three oxygens of the pendant amides and a nitrogen of the triazole.

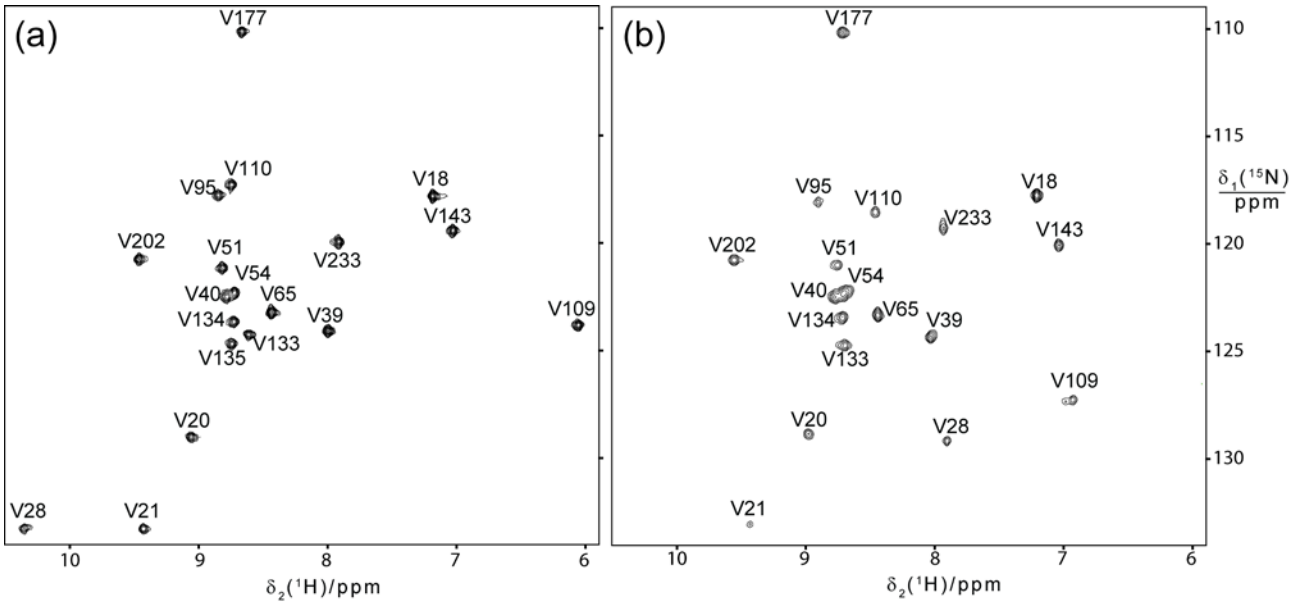

Fig. 2 ^{15}N-HSQC spectra of 0.4-0.5 mM solutions of wild-type DEBP selectively labelled with ^{15}N-valine. The spectra were recorded at 25 °C. The NMR buffer used contained 50 mM sodium phosphate, pH 7.4, and 150 mM sodium chloride. (a) Spectrum recorded in the presence of 10-fold potassium glutamate on a Bruker 800 MHz NMR spectrometer. (b) Spectrum recorded in the absence of glutamate on a Bruker 600 MHz NMR spectrometer. The cross-peaks are well resolved also at the lower magnetic field strength.

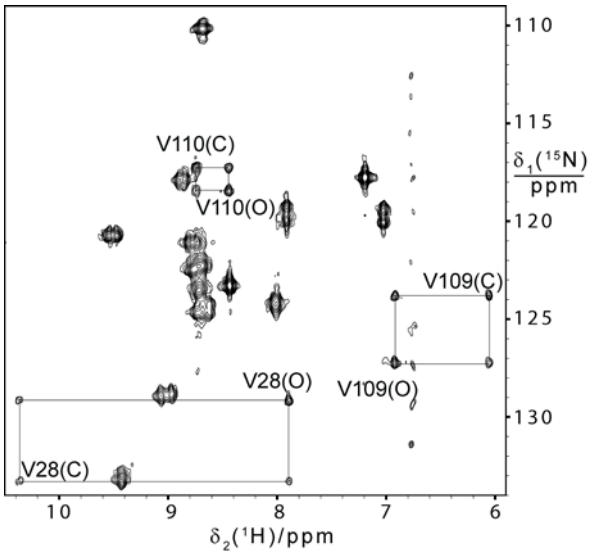

Fig. 3 Heteronuclear exchange spectroscopy experiment of an equimolar mixture of glutamate-bound and glutamate-free DEBP. The experiment was recorded at 25 ^{o}C using the experimental scheme of John et al. (2007) with a mixing time of 100 ms. The protein concentration was 0.5 mM and the total recording time 10 h. The auto peaks of V28, V109, and V110 in the glutamate-bound and glutamate-free states (see Fig. 2) are marked with an “O” and a “C”, respectively. The auto-peaks are connected by lines with the exchange cross-peaks that arise from the chemical exchange between the two states. The peak intensity ratio of the exchange cross-peaks and auto-peaks indicates an exchange rate of 7 s^{-1}.

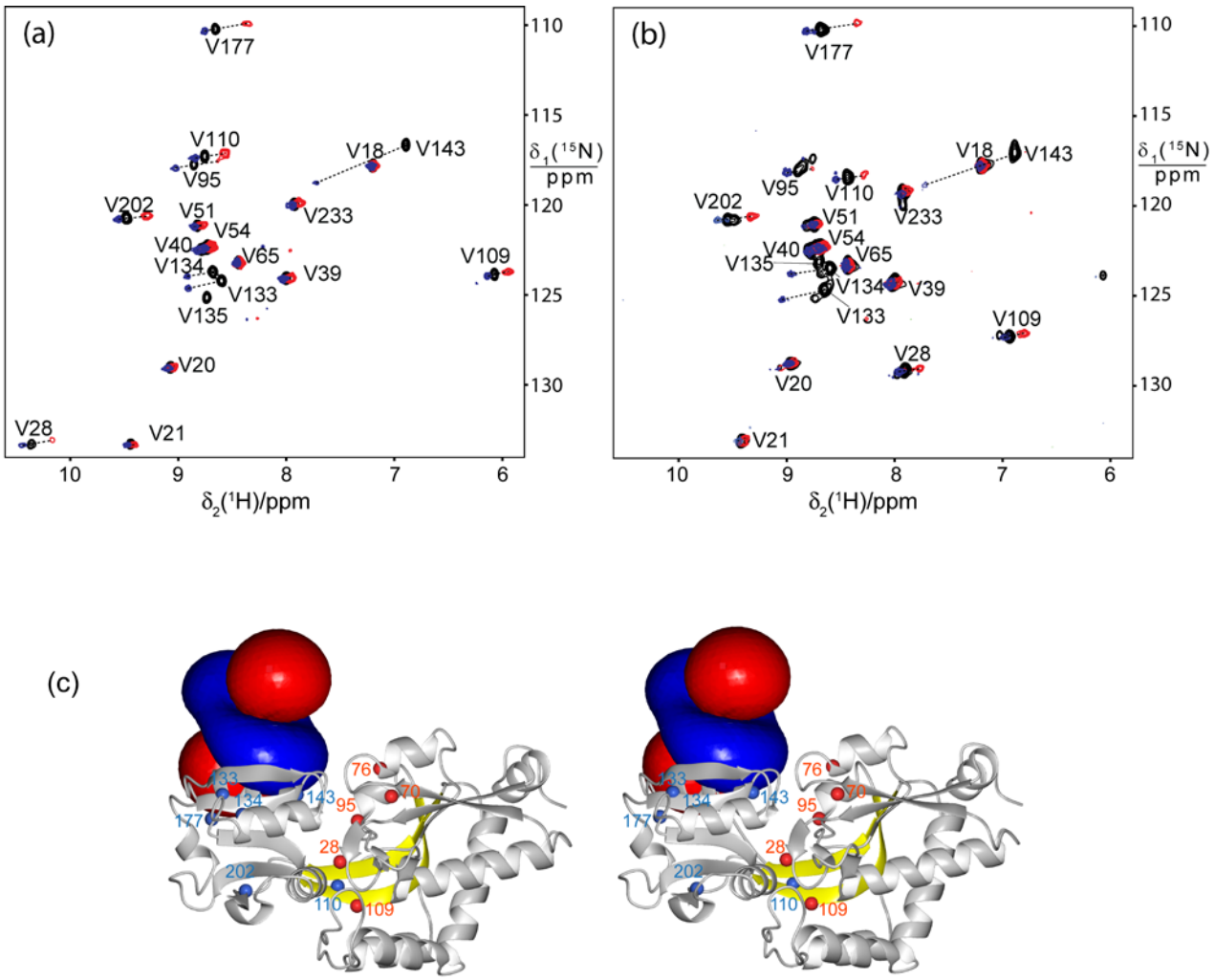

Fig. 4 Pseudocontact shifts measured for ^{15}N-valine-labelled DEBP at 25 ºC in 90% H_2O/10% D_2O. To measure PCSs, an AzF residue was incorporated in the DEBP samples at position 146 and ligated with either C3-Tm^{3+} or C3-Tb^{3+} tags. (a) ^{15}N-HSQC spectra of the glutamate-bound form. Three spectra are superimposed, with blue, red, and black cross-peaks of the samples with C3-Tm^{3+}, C3-Tb^{3+}, and untagged DEBP N146AzF, respectively. The cross-peaks are labelled with the assignment determined by site-directed mutagenesis. (b) Same as in (a), except that the ^{15}N-HSQC spectra were recorded in the absence of glutamate. (c) Stereo view of PCS isosurfaces (1 ppm in blue, -1 ppm in red) measured for Tm^{3+} in the presence of glutamate plotted on a ribbon representation of the crystal structure 2VHA (Hu et al. 2008), which is in the closed conformation. The magnetic susceptibility anisotropy ($\Delta\chi$ tensor was determined by a 5-parameter fit (axial and rhombic components and Euler angles), fixing the origin of the tensor to the location of the Gd^{3+} ion, which was established by modelling and confirmed by DEER. The locations of the amide protons for which PCSs > 0.01 ppm could be measured are indicated by blue and red balls for residues in the small and large domains, respectively. The two connecting β-strands, which define the location of the hinge for the inter-domain movement, are shown in yellow. We refer to the domains on the left and right of residue 110 as the small and large domains, respectively.

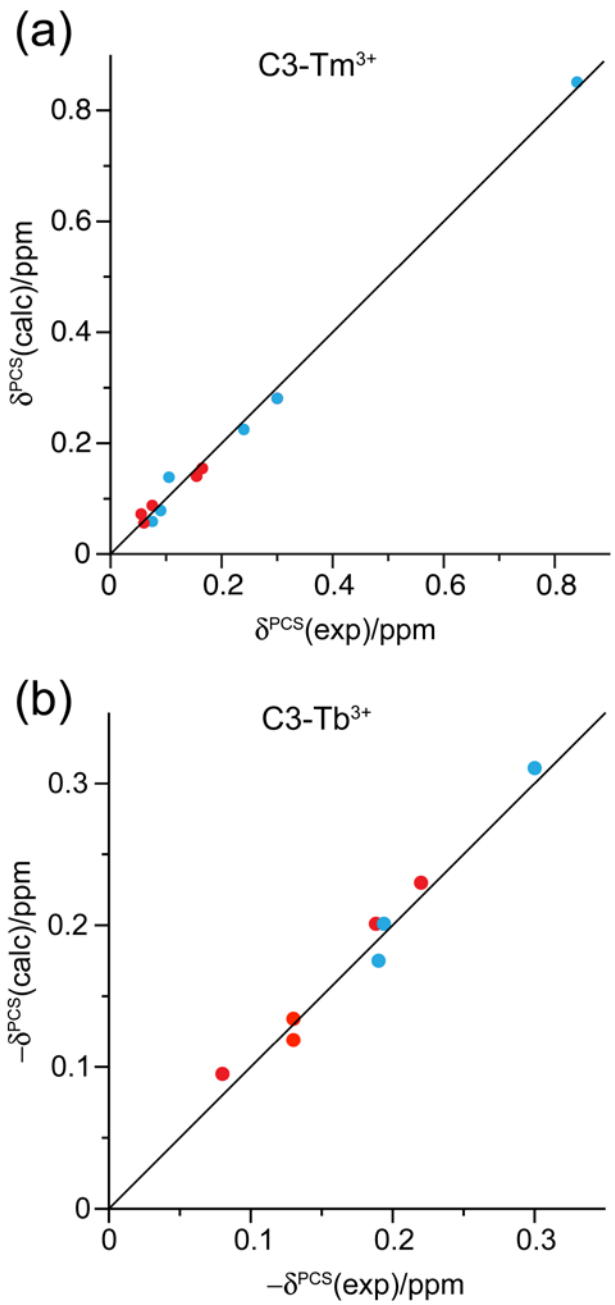

Fig. 5 Correlation between experimental and back-calculated PCSs in the presence of glutamate. Blue and red points correspond to intra-domain and inter-domain PCSs, respectively. (a) Correlation for DEBP N146AzF-C3-Tm^{3+}. The back-calculation used the 5-parameter fit to the structure 2VHA (Hu et al. 2008) with all eleven PCSs (Table S2), fixing the origin of the $\Delta\chi$ tensor at the modelled metal position (Table 1). PCSs in the small and large domain of DEBP are in blue and red, respectively. (b) Same as (a), except for DEBP N146AzF-C3-Tb^{3+}, using a 5-parameter fit with the eight PCSs of Table S3 and the modelled metal position (Table 2). Note that the axes plot negative PCSs.

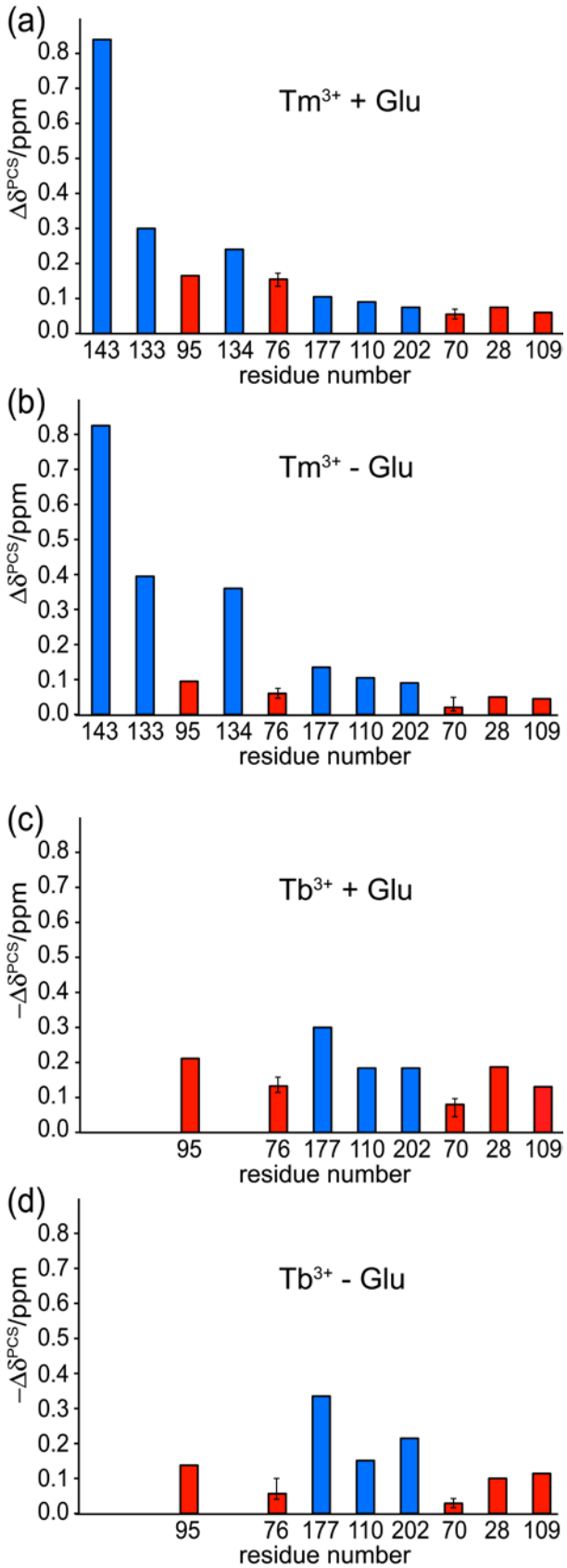

Fig. 6 Bar plots of the PCSs of amide protons of valine and isoleucine residues in DEBP N146AzF ligated with C3-Tm^{3+} or C3-Tb^{3+} tags. Blue bars identify PCSs in the small domain, while inter-domain PCSs are highlighted in red. The estimated uncertainty in PCSs is ±0.01 ppm, except for I70 and I76 for which uncertainty ranges are shown explicitly. The residues are sorted by increasing

distance of the amide protons from the metal ion (15 to 31 Å). (a) PCSs measured with the C3-Tm^{3+} tag in the presence of glutamate. (b) Same as (a), but showing the PCSs measured in the absence of glutamate. (c) PCSs measured with the C3-Tb^{3+} tag in the presence of glutamate. Note that the vertical axis displays negative PCSs to facilitate comparison with the data in (a) and (b). (d) Same as (c), but showing the PCSs measured in the absence of glutamate.